Analysis of Time-Resolved Plasma Jet Emissions That Drive Methylene Blue Dye Decomposition

Ryan P. Gott, Marisa E. Thompson, Brandon C. Staton, Brandon M. Williams, and Kunning G. Xu, *Member, IEEE*

***Abstract*— Plasma-based water purification uses energetic electrons to induce chemical reactions that break down harmful contaminants into benign components. The chemical reactions needed to decompose organic chemicals and bacteria in water are driven by the production of the hydroxyl radical, OH. In this article, an atmospheric pressure plasma jet was used to produce OH and decompose methylene blue (MB) dye in water samples. The behavior of the plasma and the emission of excited OH* near the plasma–liquid interface were analyzed. Nanosecond-resolved measurements near the plasma–water interface were obtained using ICCD imaging and emissions spectroscopy synchronized to the pulsed dc power that drives plasma formation in the plasma jet. The plasma was observed to form along the front of ionization waves as "bullets" that locally produce reactive species. When the bullet hits the water surface, it rebounds and creates a secondary excitation of species at the water surface. The bouncing phenomenon increases the plasma interactions above the water surface and increases OH* excitation up to 192%. However, this increase in excitation and emission does not necessarily mean increased total OH. Higher discharge frequencies produced more OH* emission but did not change the rate of MB dye removal. Higher voltages do increase dye removal rate but with decreasing effectiveness. The results indicate that in steady state, most of the water in the gas channel has been dissociated to form OH, and each bullet merely re-excites the ground state OH (X) into OH* (A) state. A minimum operational frequency of 1 kHz was thus found to provide the best efficiency while maintaining OH production.**

***Index Terms*— Atmospheric pressure plasma jets (APPJs), methylene blue (MB) dye, optical emission spectroscopy (OES), water purification.**

I. Introduction

With planned crewed space missions to the moon and eventually Mars, water purification with minimal consumable components, such as filters, becomes critical. Here, on Earth, nearly 30% of people lack access to clean water [1]. Today, a common purification method uses chlorine and iodine to kill certain bacteria in water. These chemicals can produce hazardous byproducts and fail to fully remove harmful contaminants and organisms. They also require replenishing consumable materials, such as chemicals and filters needed to clean the water. It is difficult to replenish these materials both in space and in many places around the world. One promising method for low consumable water purification for both in space and on Earth is the use of low-temperature plasma (LTP). By exposing water to energetic plasmas, the plasma electrons can break chemical bonds in the air near the water and in bubbles formed within the liquid to generate oxidizing species. The plasma has no consumable filter materials and typically requires high voltages but low power. Thus, plasma can provide a low-cost solution for water reuse in crewed space missions and for global water purification [2].

It is known that pulsed dc or ac atmospheric pressure plasma jets (APPJs) form as "bullets" behind an ionization wave [3]–[6]. The electric field produced at the electrode interface forms a guided streamer that propagates along the gas channel as an ionization wave of electrons. The electron-induced excitation of heavy species and their subsequent photon emissions produces the appearance of bullets in time-resolved images. Because of this behavior, the term "bullet" has been colloquially adopted to describe the phenomenon [7]–[10]. These bullets form and dissipate rapidly in accordance with the input power. Observing the bullets requires either high speed or synchronized imaging. Intensified charge-coupled device (ICCD) cameras can be synchronized to the voltage pulses that generate the plasma to observe the formation on a nanosecond timescale. Using synchronized optical emission spectroscopy (OES), the emissions of the plasma can also be observed at this timescale. While the interactions of the bullet with air have been studied at this timescale [6], [7], the interactions with water bear further exploration, particularly for water purification applications.

When LTP interacts with water, it starts the advanced oxidation process (AOP). AOP is a series of chemical reactions that kills bacteria, condenses contaminants, and purifies water. OH production is the driving force for AOP [11]. OH is primarily initiated in the plasma system by dissociation of the water molecules via impact with plasma-produced electrons or dissociative attachment

Manuscript received December 1, 2020; revised April 12, 2021; accepted June 8, 2021. Date of publication June 23, 2021; date of current version July 22, 2021. This work was supported in part by the NSF Established Program to Stimulate Competitive Research (EPSCoR) RII-Track-1 Cooperative Agreement OIA-1655280 and in part by the Alabama (AL) EPSCoR Graduate Research Scholars Program Track 14 Funding. The review of this article was arranged by Senior Editor J. L. Lopez. *(Corresponding author: Ryan P. Gott.)*

Ryan P. Gott, Brandon C. Staton, Brandon M. Williams, and Kunning G. Xu are with the Department of Mechanical and Aerospace Engineering, The University of Alabama in Huntsville, Huntsville, AL 35899 USA (e-mail: ryan.gott95@gmail.com; gabe.xu@uah.edu).

Marisa E. Thompson is with the Department of Chemistry, The University of Alabama in Huntsville, Huntsville, AL 35899 USA, and also with the Department of Mechanical and Aerospace Engineering, The University of Alabama in Huntsville, Huntsville, AL 35899 USA (e-mail: met0021@uah.edu).

Color versions of one or more figures in this article are available at https://doi.org/10.1109/TPS.2021.3089852.

Digital Object Identifier 10.1109/TPS.2021.3089852

following the reactions:

$$e^- + H_2O \rightarrow OH + H^- \quad (1)$$

$$e^- + H_2O \rightarrow OH + H + e^- \quad (2)$$

$$e^- + H_2O^+ \rightarrow OH + H. \quad (3)$$

Numerous other reactions, such as the dissociative recombination of H_3O^+, can also contribute and are described in [12]. Other products in the advanced oxidation dose, such as UV, peroxide, and ozone, can also produce more OH radicals and induce faster oxidation reaction rates [2]. While OH radicals are short-lived, they form into longer lasting species, such as peroxide, that permeate through liquid samples and provide useful reactions for purification [13]. Other species, such as ozone, can also play an important role at the interface between the plasma and the surrounding air. However, these species can be difficult to measure optically and are produced in similar quantities to OH species in air [14]. Furthermore, when interactions with water increase, OH becomes a dominant oxidative species [12]. Thus, studying the emissions of OH provides an indicator for AOP as a whole. OES can be used to observe the OH^* (A–X) transition. While it is true that the observation of this transition does not represent the entire OH inventory, at a given electron temperature, it is representative of the relative change in OH production [15].

Another species of interest for water purification is excited nitrogen. Excited nitrogen species react with OH radicals to form NO through the following reaction [16]:

$$N + OH \rightarrow NO + H. \quad (4)$$

Since this reaction is more common than the OH recombination that forms peroxide, it can detract from the OH population and can be detrimental to the AOP as a whole [17]. While these nitrogen species are beneficial for other types of plasma treatment such as plant growth, a high presence of excited nitrogen is problematic for drinking water as it can temporarily make the water more acidic. While more acidity can aid in killing bacteria [18], it is not desirable for human consumption. Since reducing the acidity requires extra steps to make the water safe to drink, it is important to understand the excitation of the nitrogen species as well, primarily to reduce them.

The use of AOP to remove contaminants has been well documented [2], [19]–[22]. One indicator that the process is working in water is the decomposition of a visible dye, such as methylene blue (MB) [23]–[25]. It has been shown that OH and O_3 are key to the decomposition of MB and that the degradation of MB in the liquid samples is directly correlated with the amount of oxidative species in the solution [26]. OH has also been shown to form peroxide, which further aids in the decomposition process [27]. It was demonstrated by Foster *et al.* [21] that spectrophotometer measurements of solution absorbance closely follow the decomposition of the contaminant. By observing the changes in coloration of a solution after various treatment times and different operating conditions, a broad understanding of the driving forces behind AOP could be developed.

The plasma bullet itself has been shown to exhibit unique behaviors when interacting with water surfaces. In models and experiments, the bullet has been observed to "bounce" off of conductive surfaces, such as water or metal [28]–[30]. The bullet deposits charge as it moves and leads to polarization of the surfaces with which it interacts. This charge build-up and polarization on the conductive target eventually leads the target to have a higher charge than the gas channel. This causes an inversion of the electric field and leads to the reverse travel of the bullet. As the bouncing bullet increases the interactions with the gas channel, there is an increase in reactive species. Observing the evolution of the emission from these species and the timing of their formation could provide a better understanding of the underlying behaviors of plasma jets used for water treatments.

In this work, an APPJ is used to provide a simple source of plasma-produced reactive species. In application, a larger system would likely be desired. However, the APPJ provides easily controllable plasma discharges that are well studied by many groups [31]–[34]. The use of an APPJ with helium gas provides a simple, scalable system that demonstrates the key trends of plasma discharges and shows important system behaviors that can be applied to larger systems. In our experiments, a pulsed dc APPJ was created using 6–10 kV of input voltage that was sufficient to induce the AOP. Parameters, such as the gas flow rate, frequency, and pulsewidth, were also varied to change the conditions and behaviors of the output plasma. A version of this design can be seen from Fig. 1(a).

II. Experimental Setup

The APPJ shown in Fig. 1(a) consists of a grounded stainless-steel box, two concentric quartz tubes (6 mm outer diameter with a 4 mm inner diameter and 2 mm outer diameter with 1 mm inner diameter) held by a nylon Tee compression fitting and a stainless-steel electrode. The outer quartz tube is 6 cm long, with 3 cm of the tube extending past the electrode. As shown in Fig. 1(b), the electrode was connected to an electrical setup consisting of an SRS DG-645 digital delay generator (DDG), a unipolar Matsusada +10-kV dc power supply, and a DEI PVX-4110 pulse generator with a rise and fall time of 60 ns. Helium gas with a purity of $>99.999\%$ was metered by a 20-slm MKS mass flow controller into the Tee.

To observe the effect of plasma treatment on water, several solutions of MB dye were made up with a concentration of $3.126e^{-5}$ M (moles per liter) in 100 mL of water. Vials containing 10-mL aliquots of these solutions were placed 1.5 cm below the jet, while the plasma was generated at different conditions. The baseline operating conditions were a voltage of 8 kV, a gas flow rate of 2-slm helium, a frequency of 6 kHz, and a pulsewidth of 1 μs. The operating parameters were then varied one at a time while holding the others constant. The MB samples were tested at voltages of 6 and 10 kV, flow rates of 1 and 3 slm, frequencies of 2 and 10 kHz, and pulsewidths of 500 ns and 2 μs. The samples were run under the plasma jet for 5, 15, 30, and 45 min. After treatment, the MB absorbance was measured using a Thermo-Scientific Genesys 10S UV-visible spectrophotometer.

The Beer–Lambert law was used to determine the concentration of MB dye and the change in concentration of the

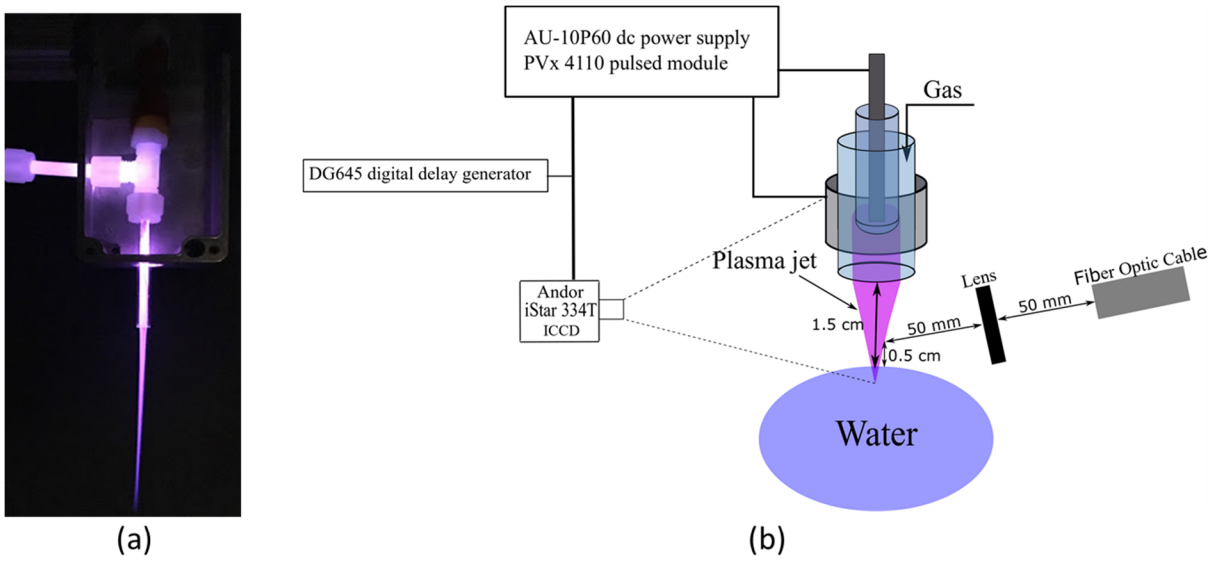

Fig. 1. APPJ (a) operating on helium and (b) experimental setup are shown.

samples. The law states

$$A = \varepsilon l c \tag{5}$$

which can be rewritten as

$$c = \frac{A}{\varepsilon l} \tag{6}$$

where A is the absorbance, ε is the molar absorptivity (L/mol · cm), l is the distance light travels through the solution (cm), and c is the concentration in mol/L. A light distance of 1 cm was used and the molar absorptivity was calculated from a measured calibration curve.

To quantify the decomposition of the dye, spectrophotometer measurements observed the UV-vis spectral absorbance of MB, as shown in Fig. 2 for the baseline condition. The peak absorbance at 666 nm was compared to the calibration curve shown in Fig. 3 to determine the percent remaining concentration at each time step. The calibration curve was calculated by measuring the absorbance of an MB solution with a starting concentration of $3.126e^{-5}$ M (moles per liter) and performing serial dilutions on this solution, down to a minimum of $2.442e^{-7}$ M. Since the light distance l is known to be 1 cm, the slope of the best fit line gives the molar absorptivity to be 44 035 L/(mol cm). For every spectrophotometer measurement of treated samples, the measured absorbance value was compared to this calibration curve to determine the MB concentration.

OES measurements were done with a 0.5-m Princeton Instruments SP2500 spectrometer coupled to a PI-MAX 4 1024 × 256 pixel ICCD camera. A fiber-optic bundle cable captured the light emissions and passed them to the spectrometer. This fiber was placed 10 cm away from the jet with a 50-mm focal length biconvex lens located halfway between the fiber and jet, as shown in Fig. 1(b). The fiber and lens were angled to capture the location 1 cm below the quartz tube. A 100 mm × 20 mm Pyrex Petri dish was placed below the plasma jet to hold the water. Experiments were run with the dish dry or with 10 mL of distilled water added.

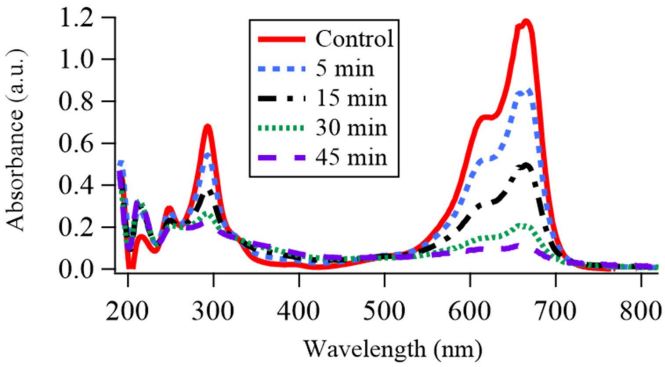

Fig. 2. UV-V is spectra measurements that show the degradation of MB dye over time for the baseline condition of 8-kV, 1000-ns, 6-kHz, and 2-slm helium flow. The starting concentration was 3.126×10^{-5} M.

With the dry dish, the plasma contacted the glass 2 cm below the APPJ tube exit. When water was present, the location of contact between the plasma and water was 1.5 cm below the tube. A 10-min warm-up time was used to bring the APPJ to steady-state operation before measurements were taken. For time-averaged measurements, the spectrometer was set to the 1200-g/mm grating, with 50 frames averaged for each measurement to improve the signal-to-noise. Each frame consisted of five charge-coupled device (CCD) accumulations to increase the signal. For synchronized measurements, ten frames were averaged and 1000 CCD images were accumulated per frame. A 3-ns gate width was used for all measurements. OH^* (A–X, 305–309.3 nm) and N_2^* second positive system ($C^3\Pi_u$–$B^3\Pi_g$, 312–320 nm) were measured. Because OH^* is a weaker emission line, multiple frames and accumulations were needed to capture the signal. An Andor iStar 334T ICCD camera was also used to capture nanosecond resolved images of the bullets. Again, a 3-ns gate width was used with an exposure time of 10 μs.

For this experiment, the plasma was observed with both synchronized images and OES to observe the differences

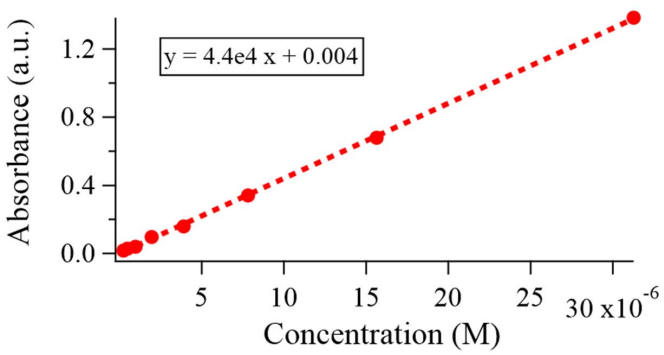

Fig. 3. Calibration curve of MB.

Fig. 4. Samples treated at 8 kV, 10 kHz, 1 μs, and 2 slm for 0, 5, 15, 30, and 45 min showed the steady degradation of MB dye.

between the plasma interacting with air and water. ICCD images were taken first to visualize the overall behavior. Time-averaged emissions were observed next to demonstrate the clear differences between these interactions. Nanosecond resolved OES measurements were then taken to show the underlying behaviors that were occurring. A list of each operating condition used for these measurements is shown in Table I. The "max" condition refers to 10 kV, 3 slm, 1 μs, and 10 kHz, as those are the individual operating conditions that lead to the most OH* emission in this system. The variations of voltage, flow rate, pulsewidth, and frequency allowed for the isolation of key physics and increased understanding of the system.

III. Results

Initial results comprised of time-averaged measurements. The decomposition of MB dye and the time-averaged reactive species emissions provided a broad look at the processes involved in water purification. Based on these results, important physical phenomena were explored with detailed time-resolved measurements. The end goal is to better understand how the time-resolved OH* species emissions correlate with the observed water purification.

A. Water Treatment

The visible degradation of MB after treatment by a single APPJ is shown in Fig. 4. Each of the samples shown was measured with the spectrophotometer. The process described in (5) and (6) was then used to determine the concentration of each sample. This was repeated for various operating conditions, producing the results shown in Fig. 5.

For all conditions, the amount of dye remaining decreased with time or, equivalently, the amount of dye removed increased. The highest voltages, frequencies, pulsewidths, and flow rates resulted in the highest rates of decomposition. The removal rate follows an exponential decay, as observed in [22].

Looking at different operating conditions, increases in voltage increase the time-averaged plasma density and temperature, which increases AOP. Higher voltages mean higher electron density [35], and thus, more OH produced based on (1)–(3). As shown in Fig. 5, the effect of voltage is not linear. There is a large increase in dye removal, from 6 to 8 kV, and only a small increase from 8 to 10 kV. This behavior indicates that there is an activation threshold for the production of OH. This is likely due to the effects of plasma contact area. At 6 kV, the jet length is shortened, and the plasma does not make direct contact with the water surface. Some reactive species still travel through the gas channel, but loss mechanisms in air will diminish the oxidative species that reach the water. Conversely, the effects of frequency and pulsewidth are minimal and mostly within error bounds. While these results show the end effect of the plasma purification of water, the underlying mechanisms that cause the variations with operating conditions needed further exploration. Thus, synchronized imaging and spectroscopy were done to help provide a broader understanding of these interactions.

B. Plasma Bullet Behavior

An analysis of ICCD images shows that the bullet forms and propagates down the helium channel, as shown in Fig. 6. This is standard behavior that has been well studied. It should be noted that the edge of the gas channel often causes the bullet to waiver near the end of its lifetime. This causes the bullet to move slightly to the left or right, as seen at 942 ns. If the bullet encounters a blockage, the ionization wave adapts to that blockage. For example, if it encounters a dry Petri dish (dielectric), it will spread radially across the surface of the dish. However, if a Petri dish filled with water is placed in the path of the channel, the bullet will rebound off the water surface and slowly move back toward the quartz tube, but never reenter the tube. This is shown in Fig. 7. The bullet will remain between the tube and the water surface for a couple of hundred nanoseconds before dissipating.

C. Time-Averaged Emission

Changes in operating conditions cause changes in reactive species emission. It should be noted that our previous study of this device showed that input power only varies with voltage and frequency [31] and thus is not specifically analyzed in this work. Fig. 8 shows the relationship between each operating condition and the wavelength integrated emission of the OH (A–X, 305-309.3 nm) transition and the N_2 second positive ($C^3\Pi_u$–$B^3\Pi_g$, 312–320 nm) transition lines. Notably, increases in voltage and frequency increase both emission intensities, while increases in flow rate decrease N_2 species

TABLE I
OPERATING CONDITIONS OF THE STEADY-STATE SPECTROSCOPY MEASUREMENTS

Condition Label	Voltage (kV)	Pulse Width (ns)	Frequency (kHz)	Flow Rate (slm)
6 kV	6	1000	6	2
8 kV	8	1000	6	2
10 kV	10	1000	6	2
500 ns	8	500	6	2
1 µs	8	1000	6	2
2 µs	8	2000	6	2
2 kHz	8	1000	2	2
6 kHz	8	1000	6	2
10 kHz	8	1000	10	2
1 slm	8	1000	6	1
2 slm	8	1000	6	2
3 slm	8	1000	6	3
Max	10	1000	10	3

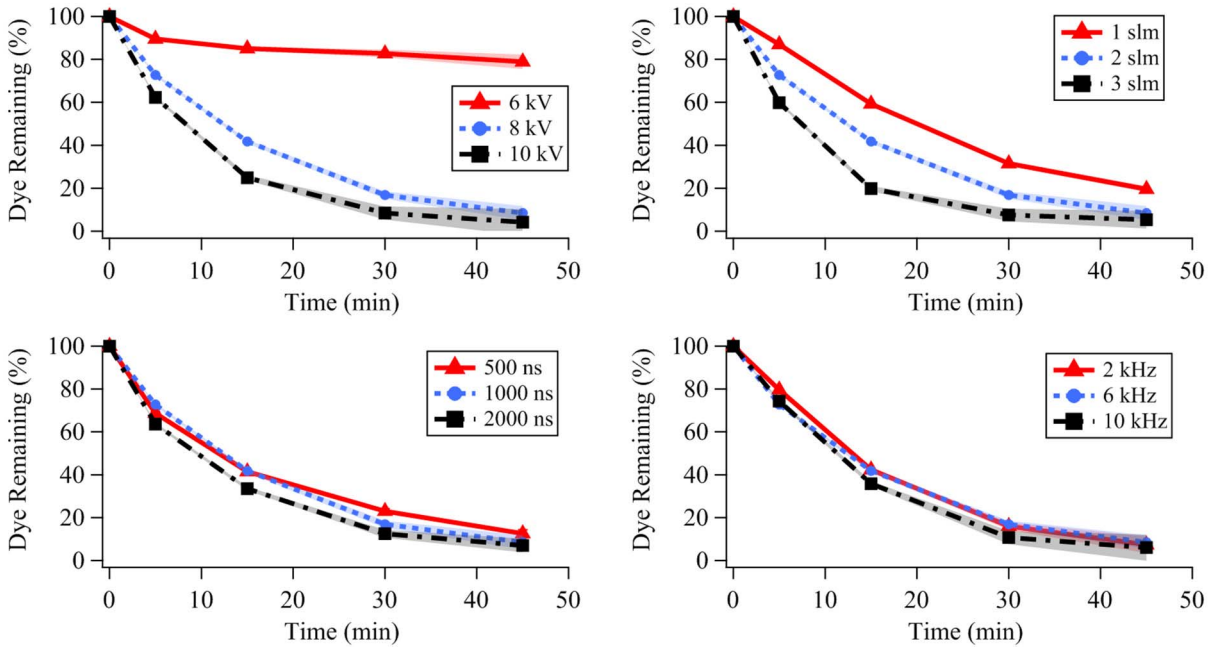

Fig. 5. Percentages of MB dye remaining after different treatment times and conditions. The baseline condition consists of 8 kV, 6 kHz, 1000 ns, and 2 slm, which is the middle value in each plot. The listed conditions represent a variation of one of these parameters. Error is shown as shading and is ±1 standard deviation.

emission and increase OH*. Higher voltage and frequency add energy to the system causing more ionization to occur in a given time frame. Higher flow rates, however, push the surrounding air out from around the tube exit, leading to a higher helium mole fraction. Because it is a molecular gas and thus has rotational and vibrational electronic energy modes, air has more energy loss mechanisms than helium. Therefore, increasing the helium mole fraction increases the ionization and production of oxidative species [36]. However, less surrounding air leads to a decrease in the nitrogen species available to be excited. With reduced nitrogen, the amount of reactive nitrogen species produced decreases. On the other hand, the moisture from the feed gas and the gas lines is still present, allowing the increased ionization to increase OH* production. Further discussion on this phenomenon is provided in our previous work [31].

The pulsewidth is unique in that the middle condition, 1 μs, produces the most reactive species emission. This is due to the lifetime of the plasma bullet. Regardless of pulsewidth, at these voltages and flow rates, the bullet itself only lasts around 1 μs. If the pulsewidth is shorter, the bullet dissipates almost immediately in synch with the trailing edge of the pulse. At that time, the electric field would dissipate, thus ending the ionization wave. This is shown in the low emission of the 500-ns case. If the pulsewidth is longer than 1 μs, the bullet has dissipated by the time the trailing edge of the pulse occurs. The rapid change in voltage at the trailing edge causes a secondary current increase that enhances the ionization of the

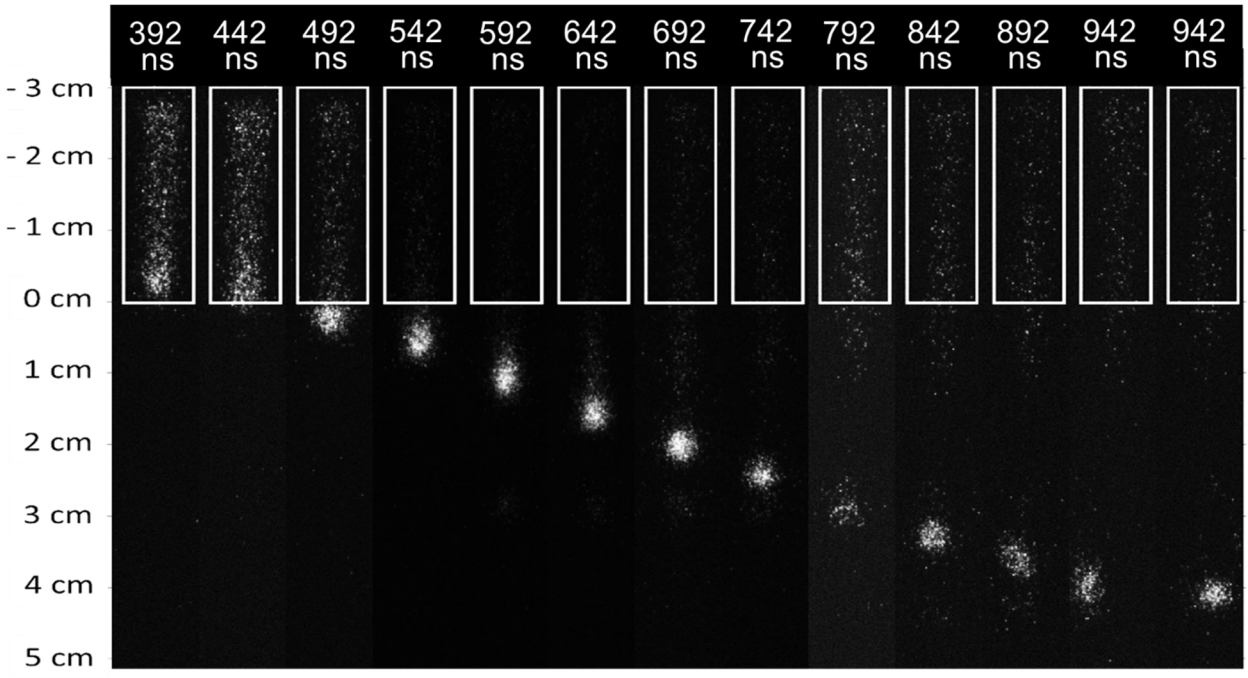

Fig. 6. Plasma forms as a bullet in correspondence with an ionization wave that travels down the helium channel. These images reflect the path of a free stream plasma jet with no obstructions.

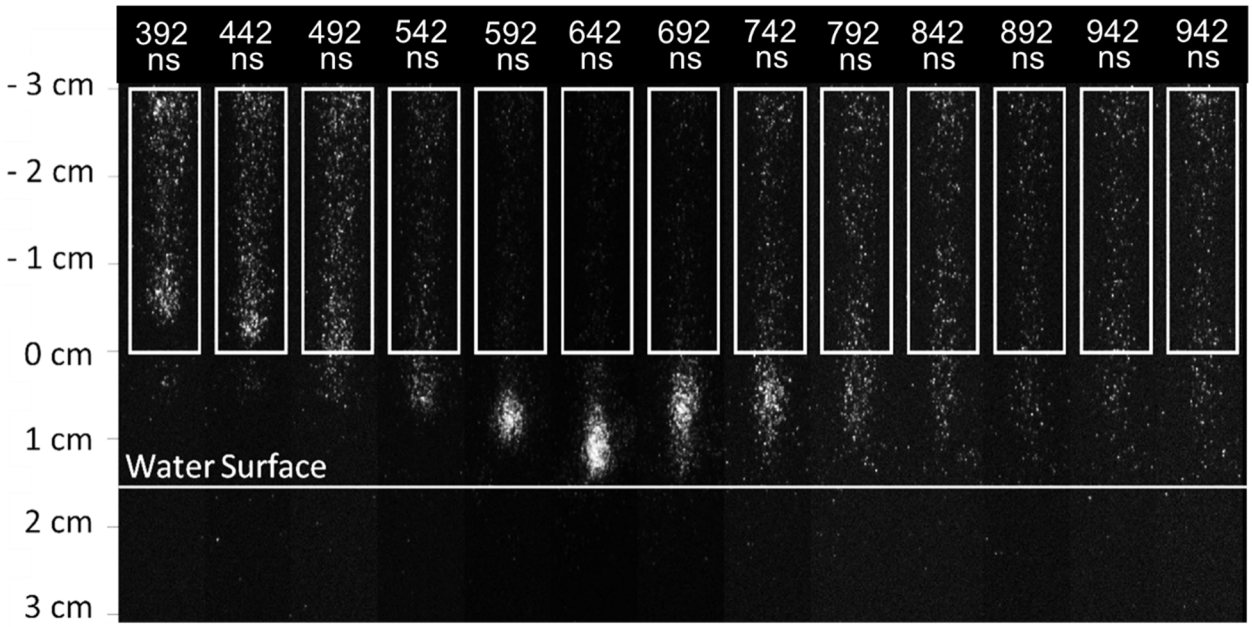

Fig. 7. Plasma bullet travels until hitting the water surface. At the interface, the bullet rebounds and starts to travel toward the tube before dissipating. The white line at 1.5 cm is the surface of the water in the dish. The baseline condition of 8 kV, 6 kHz, 1000 ns, and 2 slm is shown.

bullet. If the bullet has already dissipated, the trailing edge has less of an impact on the emissive species.

When water is added in the path of the jet, it increases the reactive species emissions. For both OH^* and excited nitrogen species, the interaction with the water surface causes an increase in emission. This is true for almost every condition, as shown in Figs. 9 and 10. Because electron interaction with water is the source of OH^* production via the reactions in (1)–(3), the increase in OH^* emission with voltage, pulsewidth, flow rate, and frequency is expected and rather significant. For the conditions tested, the emission of OH^* increased by an average of 69.6% when the plasma interacted with water. The changes ranged from a maximum of a 192% increase for the 10-kV, 3-slm, 1-μs, and 10-kHz case to a minimum of a 16.8% increase for the 6-kV case. However, an increase was also observed in the excited N_2 emissions when the plasma

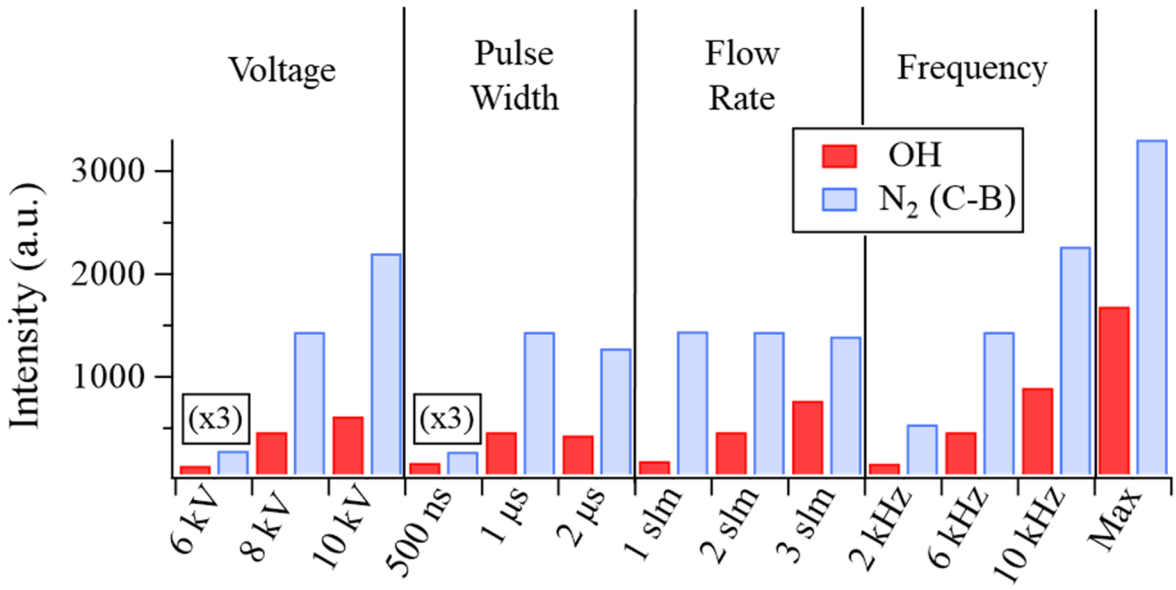

Fig. 8. Intensities of the reactive species emission change with operating conditions. The labels represent the change of one parameter from the baseline condition of 8 kV, 6 kHz, 1000 ns, and 2 slm. The max label represents the conditions of maximum emission at 10 kV, 10 kHz, 3 slm, and 1000 ns. Both the 6-kV and 500-ns condition intensities are shown multiplied by 3 to clearly see the values. The data are partitioned by operating parameter to isolate the effects of each variation.

interacts with the water. Compared to the plasma interacting with only air, the excited nitrogen species emission increased by an average of 27.4%. The changes in N_2 emissions varied from a maximum increase of 120% at 10 kV, 3 slm, 1 μs, and 10 kHz to, interestingly, a decrease of 7.5% at 1 slm. The decrease at 1 slm is likely caused by the rapid dissipation of the bullet after contacting the water. In most cases, the overall emission increase is likely due to the interactions of the ionization wave with the surface of the water. The visible plasma bullets form along an ionization wave that propagates from the electrodes down the helium channel of the jet. This ionization wave exhibits different behaviors when it hits the surface of a substrate, such as bouncing off the surface of water. This causes a secondary wave of ionization to occur.

It is interesting that a decrease in excited N_2 emissions occurs at 1 slm when water is present. At that low of a flow rate, the ionization wave does not travel far or last very long. In general, a lower flow rate leads to higher excited nitrogen emission because the bullet interacts with more air, as shown in Fig. 8 for 1–3 slm. As mentioned previously, the bullet will also have less energy at lower flow rates due to the influence of air. When the bullet hits the water surface, it rapidly dissipates due to the much higher ionization potential of liquid water compared to the surrounding gas channel. The minimal interactions that still occur are dominated by electron interaction with water, leading to more OH^* but less excited nitrogen species emission.

D. Synchronized Emission

The previous results are time-averaged OES measurements and thus are unable to distinguish between the downward and rebounding bullet. To better understand how the emissions differ when plasma is interacting with the water surface, spectroscopic measurements were taken at nanosecond increments in synch with the voltage pulse. This resulted in emission plots like Fig. 10 for each time step. These were then integrated with respect to wavelength to isolate the total intensity of OH^* (305–309.3 nm) and excited N_2 emissions (311–318 nm), resulting in the plots shown in Fig. 11. The integration limits were chosen to capture as much of each excited state without overlapping. An analysis of how operating conditions affect the emissions over the lifetime of the bullet was conducted in our previous work [37]. We found that a higher voltage increases the initial emission peak value and causes the peak to occur sooner in time. Flow rate also had an effect. Higher flow rates had higher peak emissions, but the peak occurred later compared to lower flow rates. This was due to a mixture of preseeding and temperature effects.

In this work, these effects can be seen from Fig. 11. From the observations shown in Fig. 8, it was evident that higher voltages and flow rates are desirable for increasing OH^*. Higher frequencies are also beneficial for OH^* emission, but since synchronized imaging only observes individual bullets, the frequency, which is a measure of how many bullets occur per second, would not have an immediate effect. Thus, the case of 10-kV voltage, 3-slm helium flow rate was compared to the 2 slm, 10 kV, and the 3 slm, 8-kV cases with the frequency and pulsewidth remaining at the baseline (6 kHz, 1000 ns). Voltage has the largest effect on emissions. Both 10-kV cases demonstrate peaks 50% higher with no water and twice as high with water compared to the 8-kV case. The higher voltage also increases the velocity of the bullet, causing the emission peaks to occur sooner in time. Flow rate does not have a significant effect but does allow OH to sustain longer. This is likely because there are many loss mechanisms for OH in air [38]. With higher flow rates, the gas channel has more helium and less air, which slows the rate of OH decomposition. When water is present, the higher flow rate also causes more

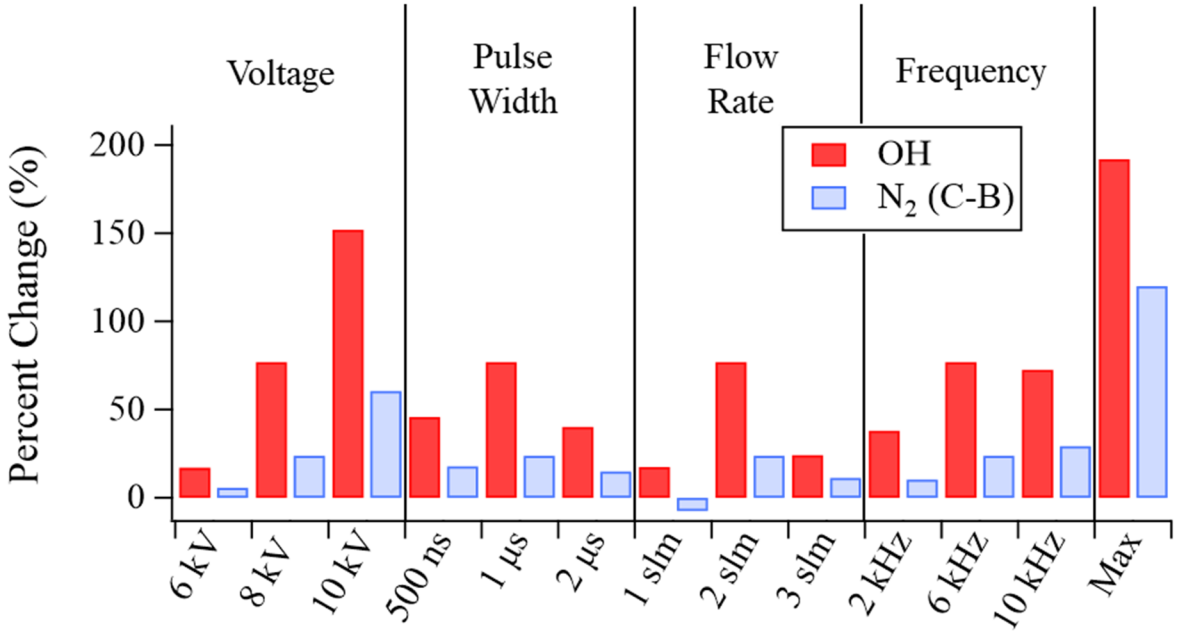

Fig. 9. Percent difference between the plasma emissions with water versus the emissions without water interaction is shown. The labels represent the change of one parameter from the baseline condition of 8 kV, 6 kHz, 1000 ns, and 2 slm. The max label represents the conditions of maximum emission at 10 kV, 10 kHz, 3 slm, and 1000 ns. The data are partitioned by operating parameter to isolate the effects of each variation.

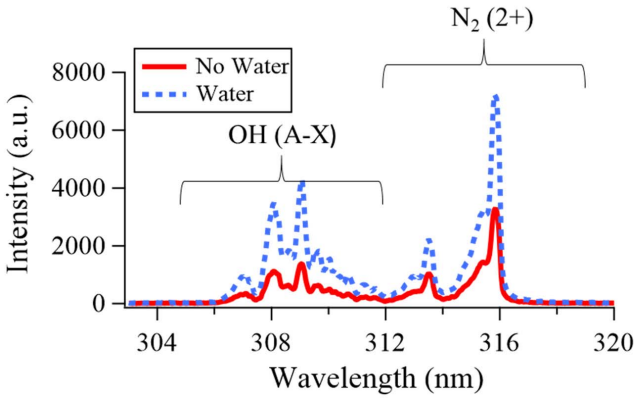

Fig. 10. Reactive species at the plasma–water interface (1.5 cm below the tube exit) increase when plasma interacts with water as opposed to air. The conditions of maximum emission at 10 kV, 10 kHz, 3 slm, and 1000 ns are shown.

water to turn into vapor and enter the gas channel, causing an increase in OH* emissions.

When interacting with water, another unique behavior occurs. For the N_2 species emission, a larger secondary peak rapidly appears after the initial peak in emissions. A secondary peak also occurs for OH* but immediately follows and is nearly equal in magnitude to the first peak. The presence of the secondary peak is likely due to increased plasma interactions. As the plasma bullet hits a water surface, it rebounds and then stalls in place before dissipating, as shown in Fig. 7. The presence of the ionization wave will both produce more species and excite existing species. It should be noted that the voltage drives the velocity of the bullet. Thus, the 3-slm and 8-kV data shown in Fig. 11 match the timing shown in Figs. 6 and 7, while the 10-kV data show faster propagation.

IV. Discussion

A. OH Emissions Versus OH Population for Dye Decomposition

The rates of decomposition of MB dye most strongly correlate to changes in voltage and flow rate. Pulsewidth and frequency did not have a significant effect. Higher voltages and flow rates increased the rate of dye decomposition and also increased reactive species emission. On the contrary, higher frequencies also significantly increased the time-averaged reactive species emission but did not have a large effect on MB dye decomposition. Since OH is a driving force for AOP and increased AOP reactions would reduce more dye, this discrepancy indicates that the emission of OH* is not a direct indicator of the total amount of OH.

Under the assumption that (1)–(3) account for most of the OH inventory [ions come from (2)], the production rate of OH is given by

$$\frac{dn_{\mathrm{OH}}}{dt} = (k_{\mathrm{OH+}} + k_{\mathrm{OH-}} + k_{\mathrm{OH(X)}} + k_{\mathrm{OH(A)}})n_e n_{\mathrm{H_2O}} + (k_{\mathrm{OH+}} + k_{\mathrm{OH-}} + k_{\mathrm{OH(X)}} + k_{\mathrm{OH(A)}})n_e n_{\mathrm{H_2O+}} \quad (7)$$

where k are the rate coefficients for the production of positive and negative ions, ground state OH, and excited A state OH, n_e is the electron density, and n_{H2O} is the water number density. It is assumed that the OH ions will neutralize and can be counted into the total OH inventory. The dissociation of water can produce either ground state OH (X) or excited state OH* (A), and the latter radiatively decays to the ground state and produces the characteristic A–X transition of OH. The total OH inventory must include both ground state and excited OH*, but only the emission from OH* can be measured with OES.

While higher frequencies would indicate more electron interactions per second, there are a limited number of H_2O

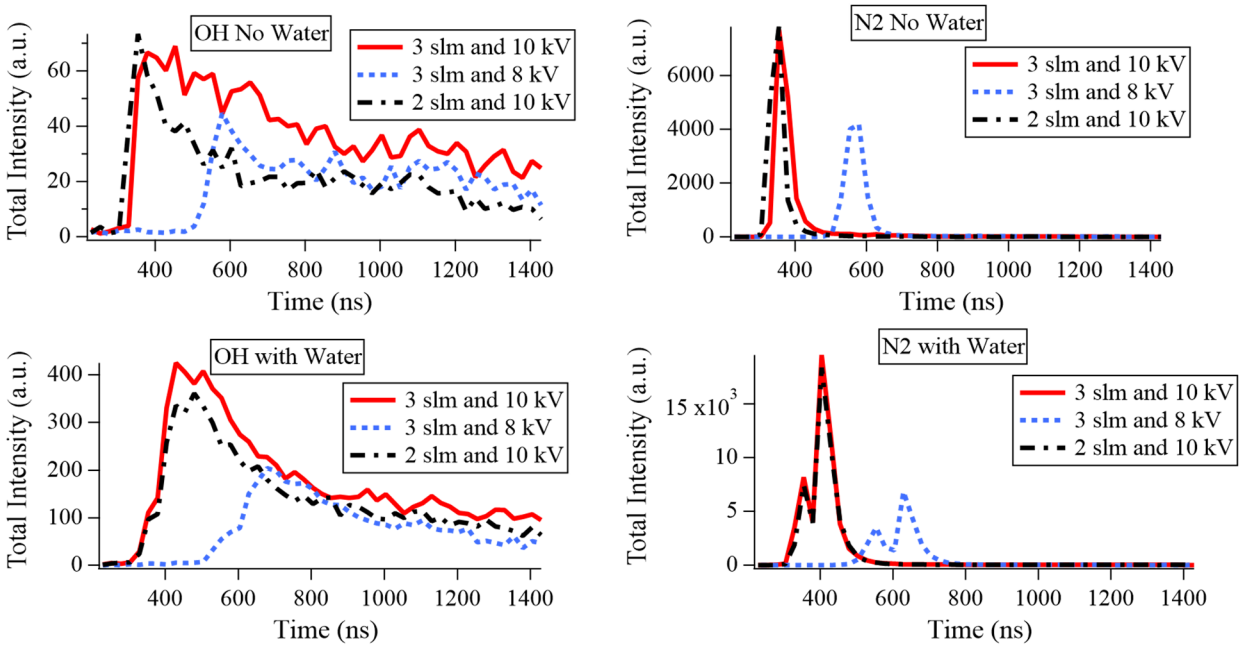

Fig. 11. Synchronized spectroscopic measurements provide a nanosecond resolved look at the plasma emissions 1.5 cm below the tube exit.

molecules. At 2 slm, the flow velocity is about 2.7 m/s. This means that a slug of gas takes about 17 ms to travel the 4.5 cm from the pin to the water surface, which is orders of magnitude longer than the time between bullets at these frequencies (100–500 μs). Thus, once the water molecules in the gas channel are dissociated into OH, few water molecules will be available to further produce OH. While the lifetime of the OH molecules is also around hundreds of microseconds [39], the molecules will combine into other chemical species, such as peroxide or NO. Since these reactions will use H and O atoms, this will prevent the formation of H_2O and reduce the overall water number density. The reactions noted in (1)–(3) show that the production of OH depends on the electron density, electron temperature (through the rate constant), and water number density. The electron temperature and density do not change between bullets, and thus, no additional OH will be formed until the water number density increases.

The observed emissions represent the (A–X) transition for OH. This means that when emissions are observed, the A state of OH has relaxed back to the ground state. The excitation and decay processes together last on the order of single microseconds. Since the time between bullets is from 500 to 100 μs for the frequency ranges of 2–10 kHz, the A state excitation process will occur more often per second at high frequencies. In the time between pulses, the states generated in (7) will mostly decay back to the X state. Thus, with no new H_2O molecules when the next bullet occurs, the electrons primarily excite OH via

$$\frac{dn_{\mathrm{OH}}(A)}{dt} = k_{\mathrm{OH(A)}} n_e n_{\mathrm{OH(X)}}. \tag{8}$$

Then, we observe the resulting radiative decay with OES. Thus, more bullets result in more time-average emissions, but not more OH molecules. Essentially, once all the H_2O molecules have been dissociated into OH, the plasma bullets simply reexcite the same population of OH. At higher voltages, the increase in electron temperature increases the rate coefficient in (7) and (8) [15], [40], thus increasing the amount of overall OH produced and the amount excited. Increases in flow rate will increase the velocity of the bulk flow. This will allow new water molecules to interact with the electrons sooner, thus increasing the overall OH inventory. At the nanosecond time scale that these reactions are occurring, it is difficult to separate these two reactions. For future studies, advanced fast laser techniques are needed to isolate the precise populations of each state.

B. Frequency Limit

The limitation of the effects of frequency implies that there is a minimum frequency that the plasma jet can be operated at to still maintain effective treatment. Finding this minimum frequency would improve the efficiency of the treatment process. Additional testing was thus performed to identify the limit of frequency effects. Using the baseline parameters of 8 kV, 2 slm, and 1 μs, the frequency was varied from 10 kHz to 1 Hz. The largest differences in Fig. 5 between frequencies are shown to be near 15 min of treatment. Thus, each sample was treated for 15 min at each frequency and the results are shown in Fig. 12.

The minimum frequency before losses in dye removal rate begin to occur is around 1 kHz. At this frequency, there is 1 ms between each bullet. At this time scale, some of the gas flow will have started replenishing and some of the OH molecules will have recombined into H_2O but not enough to largely affect the performance. Below 1 kHz, the time between bullets increases and more and more molecules are lost between bullets without dissociating into OH, which reduces

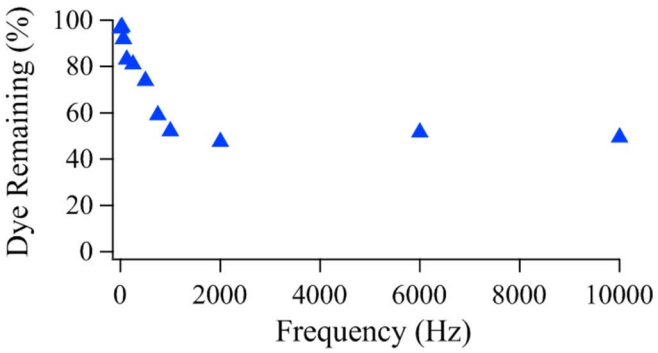

Fig. 12. Variations in dye removal with changes in frequency at 15-min treatment times. The plasma was operated at an 8-kV voltage, 2-slm helium flow rate, and 1-μs pulsewidth.

dye removal. In addition, since the bullet travels 4.5 cm from the pin to the water surface, preseeding effects will start to play a role at this timescale. Higher pulse frequencies create a path of ionization that allows the bullet to follow an easily ionized channel [37]. As the frequency decreases, this preseeded channel weakens, and more loss mechanisms occur. Both the gas channel replenishment timing and the preseeding effects imply that the minimum frequency would reduce if the distance between the jet and the water was shortened.

Notably, the difference in dye removal between 10 and 1 kHz is 2.6% (49.4% remaining versus 52.0%). However, the current draw, which is linear with frequency, sees an order of magnitude reduction from 36 to 3.6 W [31]. This means that the efficiency of plasma-based purification devices can be greatly improved by operating at this minimum frequency.

C. Bullet–Water Interactions

Interacting with water also causes a significant increase in OH. Since the electron temperature and density do not change on a bullet by bullet basis, an increase in emission at identical operating conditions indicates that there is more OH to be excited. The water number density increases due to the stirring of water into the gas channel, and this is likely the main cause of the overall increase in OH^* emission with water. In addition, an increase in electron density has been observed in both models and experiments when ionization waves interact with conductive surfaces [28], [41].

The emission behaviors seen in Figs. 9 and 11 with and without water are directly related to the rebounding bullet phenomenon in Fig. 7. It should be noted that the bullet rebounding behavior is likely due to polarization caused by charge buildup on the water surface. Further discussion of this behavior is provided in the literature [28], [42]. The initial bullet pass causes a spike in emission followed by a standard rate of decay. The plots show that without water, the excitation times (rise in emissions) for both OH^* and excited nitrogen species are between 25 and 50 ns for all conditions. The decay time for the nitrogen species is also around 25–50 ns, while OH^* decays over 1 μs. The excitation and decay times remain the same when water is present, indicating that the chemical/excitation process is the same for the primary bullet and the secondary rebound bullet.

Notably, the bullet bounce causes a secondary peak in emissions that increases N_2 excitation. The secondary peaks show the same excitation and decay times as the initial peaks. The magnitude of the secondary peak is significant, as it is larger than the initial peak. Two factors likely cause this increase. First, the initial decay process has already begun. Some of the decayed molecules will be reexcited when the bullet rebounds. Also, when the bullet passes through space, some electrons are temporarily left in the previously traveled path. When the bullet rebounds, the ionization wave travels back into that cloud of electrons and briefly causes an increase in electron density, leading to the high secondary peak of N_2 species emission. This dissipates before the next bullet is generated, leading to a consistently lower magnitude for the first peak.

V. Conclusion

The interactions between a plasma bullet and water show useful chemical reactions for water treatment. These interactions help explain why increasing voltage and flow rate increase the rate of decomposition of contaminants such as MB dye. In most cases, the presence of water causes an increase in emissive species. The plasma bullet will rebound off the water surface causing a large secondary peak in emissive species. However, the increased emission does not mean more actual production of OH due to the long lifetime of OH compared to the lifetime of bullets. Higher frequencies do not help in the overall goal of cleaning water, so lower frequencies (down to 1 kHz), and thus lower input powers, can be utilized.

To progress this work, a few main areas need to be explored. The first is modeling. The spatiotemporal evolution of the emissions that were observed here will aid in modeling the behaviors of the plasma and its interaction with water. Models are needed to demonstrate how the gas phase kinetics affects the rebound of the bullet and how the water is affected by these changes. Finally, the plasma itself needs to be expanded. Developing a larger surface area plasma has long been a challenge in the LTP field, and any development toward this goal will benefit water treatment.

References

[1] *Results of Round I of the WHO International Scheme to Evaluate Household Water Treatment Technologies*, I. Com, World Health Org., Geneva, Switzerland, 2016.

[2] J. Foster, B. S. Sommers, S. N. Gucker, I. M. Blankson, and G. Adamovsky, "Perspectives on the interaction of plasmas with liquid water for water purification," *IEEE Trans. Plasma Sci.*, vol. 40, no. 5, pp. 1311–1323, May 2012.

[3] M. Teschke, J. Kedzierski, E. G. Finantu-Dinu, D. Korzec, and J. Engemann, "High-speed photographs of a dielectric barrier atmospheric pressure plasma jet," *IEEE Trans. Plasma Sci.*, vol. 33, no. 2, pp. 310–311, Apr. 2005.

[4] X. Lu and M. Laroussi, "Dynamics of an atmospheric pressure plasma plume generated by submicrosecond voltage pulses," *J. Appl. Phys.*, vol. 100, no. 6, Sep. 2006, Art. no. 063302.

[5] Y. Xian *et al.*, "On plasma bullet behavior," *IEEE Trans. Plasma Sci.*, vol. 37, no. 10, pp. 2068–2073, Oct. 2009.

[6] X. Lu, G. V. Naidis, M. Laroussi, and K. Ostrikov, "Guided ionization waves: Theory and experiments," *Phys. Rep.*, vol. 540, no. 3, pp. 123–166, Jul. 2014.

[7] M. Laroussi, "Low-temperature plasma jet for biomedical applications: A review," *IEEE Trans. Plasma Sci.*, vol. 43, no. 3, pp. 703–712, Mar. 2015.

[8] X. Lu, M. Laroussi, and V. Puech, "On atmospheric-pressure non-equilibrium plasma jets and plasma bullets," *Plasma Sources Sci. Technol.*, vol. 21, no. 3, Jun. 2012, Art. no. 034005.
[9] L. Ji, Y. Xia, Z. Bi, J. Niu, and D. Liu, "The density and velocity of plasma bullets propagating along one dielectric tube," *AIP Adv.*, vol. 5, no. 8, Aug. 2015, Art. no. 087181.
[10] B. L. Sands, B. N. Ganguly, and K. Tachibana, "Time-resolved imaging of 'plasma bullets' in a dielectric capillary atmospheric pressure discharge," *IEEE Trans. Plasma Sci.*, vol. 36, no. 4, pp. 956–957, Aug. 2008.
[11] J. L. Wang and L. J. Xu, "Advanced oxidation processes for wastewater treatment: Formation of hydroxyl radical and application," *Crit. Rev. Environ. Sci. Technol.*, vol. 42, no. 3, pp. 251–325, Feb. 2012.
[12] P. Bruggeman and D. C. Schram, "On OH production in water containing atmospheric pressure plasmas," *Plasma Sources Sci. Technol.*, vol. 19, no. 4, Aug. 2010, Art. no. 045025.
[13] N. K. Kaushik *et al.*, "Biological and medical applications of plasma-activated media, water and solutions," *Biol. Chem.*, vol. 400, no. 1, pp. 39–62, Dec. 2018.
[14] Y. Liu, D. Liu, J. Zhang, B. Sun, A. Yang, and M. G. Kong, "1D fluid model of RF-excited cold atmospheric plasmas in helium with air gas impurities," *Phys. Plasmas*, vol. 27, no. 4, Apr. 2020, Art. no. 043512.
[15] Y. Itikawa and N. Mason, "Cross sections for electron collisions with water molecules," *J. Phys. Chem. Reference Data*, vol. 34, no. 1, pp. 1–22, Mar. 2005.
[16] H. S. Uhm, "Generation of various radicals in nitrogen plasma and their behavior in media," *Phys. Plasmas*, vol. 22, no. 12, Dec. 2015, Art. no. 123506.
[17] B. Ghimire *et al.*, "Enhancement of hydrogen peroxide production from an atmospheric pressure argon plasma jet and implications to the antibacterial activity of plasma activated water," *Plasma Sources Sci. Technol.*, vol. 30, no. 3, Mar. 2021, Art. no. 035009.
[18] P. Shaw *et al.*, "Bacterial inactivation by plasma treated water enhanced by reactive nitrogen species," *Sci. Rep.*, vol. 8, no. 1, pp. 1–10, Dec. 2018.
[19] I. Even-Ezra, A. Mizrahi, D. Gerrity, S. Snyder, A. Salveson, and O. Lahav, "Application of a novel plasma-based advanced oxidation process for efficient and cost-effective destruction of refractory organics in tertiary effluents and contaminated groundwater," *Desalination Water Treatment*, vol. 11, nos. 1–3, pp. 236–244, Nov. 2009.
[20] N. Wardenier, P. Vanraes, A. Nikiforov, S. W. H. Van Hulle, and C. Leys, "Removal of micropollutants from water in a continuous-flow electrical discharge reactor," *J. Hazardous Mater.*, vol. 362, pp. 238–245, Jan. 2019.
[21] J. E. Foster, G. Adamovsky, S. N. Gucker, and I. M. Blankson, "A comparative study of the time-resolved decomposition of methylene blue dye under the action of a nanosecond repetitively pulsed DBD plasma jet using liquid chromatography and spectrophotometry," *IEEE Trans. Plasma Sci.*, vol. 41, no. 3, pp. 503–512, Mar. 2013.
[22] J. E. Foster, S. Mujovic, J. Groele, and I. M. Blankson, "Towards high throughput plasma based water purifiers: Design considerations and the pathway towards practical application," *J. Phys. D: Appl. Phys.*, vol. 51, no. 29, Jul. 2018, Art. no. 293001.
[23] J.-L. Brisset *et al.*, "Chemical reactivity of discharges and temporal post-discharges in plasma treatment of aqueous media: Examples of gliding discharge treated solutions," *Ind. Eng. Chem. Res.*, vol. 47, no. 16, pp. 5761–5781, Aug. 2008.
[24] H. Aoki, K. Kitano, and S. Hamaguchi, "Plasma generation inside externally supplied ar bubbles in water," *Plasma Sources Sci. Technol.*, vol. 17, no. 2, May 2008, Art. no. 025006.
[25] L. Chandana, P. M. K. Reddy, and C. Subrahmanyam, "Atmospheric pressure non-thermal plasma jet for the degradation of methylene blue in aqueous medium," *Chem. Eng. J.*, vol. 282, pp. 116–122, Dec. 2015.
[26] F. Huang, L. Chen, H. Wang, and Z. Yan, "Analysis of the degradation mechanism of methylene blue by atmospheric pressure dielectric barrier discharge plasma," *Chem. Eng. J.*, vol. 162, no. 2, pp. 250–256, 2010. Accessed: Sep. 28, 2020. [Online]. Available: https://reader.elsevier.com/reader/sd/pii/S1385894710004808?token=3A4FB637E76CB96C5C666F8C09D8A52EC59E8F69B32EDAE834768085347FD8996A44881F25D4706A39212FD64BA5AD4C
[27] M. C. García *et al.*, "Microwave atmospheric pressure plasma jets for wastewater treatment: Degradation of methylene blue as a model dye," *Chemosphere*, vol. 180, pp. 239–246, Aug. 2017.
[28] N. Y. Babaeva *et al.*, "Plasma bullet propagation and reflection from metallic and dielectric targets," *Plasma Sources Sci. Technol.*, vol. 28, no. 9, Sep. 2019, Art. no. 095006.
[29] V. V. Kovačević, G. B. Sretenović, E. Slikboer, O. Guaitella, A. Sobota, and M. M. Kuraica, "The effect of liquid target on a nonthermal plasma jet—Imaging, electric fields, visualization of gas flow and optical emission spectroscopy," *J. Phys. D: Appl. Phys.*, vol. 51, no. 6, Jan. 2018, Art. no. 065202.
[30] T. Darny, J. M. Pouvesle, J. Fontane, L. Joly, S. Dozias, and E. Robert, "Analysis of conductive target influence in plasma jet experiments through helium metastable and electric field measurements," *Plasma Sources Sci. Technol.*, vol. 26, no. 10, Sep. 2017, Art. no. 105001.
[31] R. P. Gott and K. G. Xu, "OH production and jet length of an atmospheric-pressure plasma jet for soft and biomaterial treatment," *IEEE Trans. Plasma Sci.*, vol. 47, no. 11, pp. 4988–4999, Nov. 2019.
[32] M. Boselli *et al.*, "Characterization of a cold atmospheric pressure plasma jet device driven by nanosecond voltage pulses," *IEEE Trans. Plasma Sci.*, vol. 43, no. 3, pp. 713–725, Mar. 2015.
[33] M. Pinchuk, O. Stepanova, N. Kurakina, and V. Spodobin, "Propagation of atmospheric pressure helium plasma jet into ambient air at laminar gas flow," *J. Phys., Conf. Ser.*, vol. 830, May 2017, Art. no. 012060.
[34] K. Niemi, S. Reuter, L. Schaper, N. Knake, V. Schulz-Von Der Gathen, and T. Gans, "Diagnostics on an atmospheric pressure plasma jet," *J. Phys., Conf. Ser.*, vol. 71, no. 1, 2007, Art. no. 012012.
[35] M. A. Naveed, N. U. Rehman, S. Zeb, S. Hussain, and M. Zakaullah, "Langmuir probe and spectroscopic studies of RF generated helium-nitrogen mixture plasma," *Eur. Phys. J. D*, vol. 47, no. 3, pp. 395–402, May 2008.
[36] E. Karakas, M. Koklu, and M. Laroussi, "Correlation between helium mole fraction and plasma bullet propagation in low temperature plasma jets," *J. Phys. D: Appl. Phys.*, vol. 43, no. 15, Apr. 2010, Art. no. 155202.
[37] R. P. Gott and K. G. Xu, "Time-resolved imaging and spectroscopy of atmospheric pressure plasma bullet propagation and RONS production," *J. Phys. D: Appl. Phys.*, vol. 53, no. 31, Jul. 2020, Art. no. 315201.
[38] J. T. Herron and D. S. Green, "Chemical kinetics database and predictive schemes for nonthermal humid air plasma chemistry. Part II. Neutral species reactions," *Plasma Chem. Plasma Process.*, vol. 21, no. 3, pp. 459–481, 2001.
[39] C. G. Parigger, C. M. Helstern, B. S. Jordan, D. M. Surmick, and R. Splinter, "Laser-plasma spectroscopy of hydroxyl with applications," *Molecules*, vol. 25, no. 4, p. 988, Feb. 2020.
[40] K. Chakrabarti, V. Laporta, and J. Tennyson, "Calculated cross sections for low energy electron collision with OH," *Plasma Sources Sci. Technol.*, vol. 28, no. 8, Aug. 2019, Art. no. 085013.
[41] B. L. M. Klarenaar, O. Guaitella, R. Engeln, and A. Sobota, "How dielectric, metallic and liquid targets influence the evolution of electron properties in a pulsed he jet measured by Thomson and Raman scattering," *Plasma Sources Sci. Technol.*, vol. 27, no. 8, Aug. 2018, Art. no. 085004.
[42] A. Koné, F. P. Sainct, C. Muja, B. Caillier, and P. Guillot, "Investigation of the interaction between a helium plasma jet and conductive (metal)/non-conductive (dielectric) targets," *Plasma Med.*, vol. 7, no. 4, pp. 333–346, 2017.

Ryan P. Gott received the B.S. and M.S. degrees in aerospace engineering from The University of Alabama in Huntsville, Huntsville, AL, USA, in 2016 and 2018, respectively, where he is currently pursuing the Ph.D. degree with the Mechanical and Aerospace Engineering Department.

His research interests include the study of atmospheric plasmas and their applications to plant, water, and biomaterial treatment.

Marisa E. Thompson received the B.S. degree in chemistry from The University of Alabama in Huntsville, Huntsville, AL, USA, in 2020, where she is currently pursuing the M.S. degree in chemistry.

Her research interests include organic chemistry, polymer synthesis, and using chemistry to find environmentally friendly methods of performing necessary processes.

Brandon C. Staton is currently pursuing the B.S. degree in the aerospace engineering program with The University of Alabama in Huntsville, Huntsville, AL, USA.

His research interests include the study of pulsed plasma jets and plasma propulsion.

Brandon M. Williams received the B.S. degree in mechanical engineering from The University of Alabama in Huntsville, Huntsville, AL, USA, in 2020.

His research interests include the study of thermonuclear fusion plasma dynamics and atmospheric-pressure plasma fluid dynamics.

Kunning G. Xu (Member, IEEE) received the B.S., M.S., and Ph.D. degrees in aerospace engineering from the Georgia Institute of Technology, Atlanta, GA, USA, in 2006, 2009, and 2012, respectively.

He is currently an Associate Professor with the Mechanical and Aerospace Engineering Department, The University of Alabama in Huntsville, Huntsville, AL, USA. His research interests include plasma propulsion, plasma-assisted combustion, and atmospheric-pressure microplasma science and engineering.